Two-body photodisintegration of ^{4}He in the 100–360 MeV region

R. A. Schumacher,* J. L. Matthews, W. W. Sapp, and R. S. Turley†
Department of Physics and Laboratory for Nuclear Science, Massachusetts Institute of Technology, Cambridge, Massachusetts 02139

G. S. Adams
Department of Physics and Astronomy, University of South Carolina, Columbia, South Carolina 29208

R. O. Owens
Department of Natural Philosophy, University of Glasgow, Glasgow, Scotland
(Received 1 July 1985)

Measurements of the differential cross sections for the ^{4}He(γ,n)^{3}He and ^{4}He(γ,p)^{3}H reactions have been performed for photon energies in the 100–360 MeV region. Results were obtained for nucleon center-of-mass angles close to 60°, 90°, and 120° by detecting the recoiling nuclei with a magnetic spectrometer. Both (γ,p) and (γ,n) cross sections are forward peaked and fall rapidly as a function of photon energy. The (γ,p) to (γ,n) cross section ratio is in the range 0.7–1.3 at each angle and tends to increase with photon energy. The data are compared with a calculation by Gari and Hebach which includes meson exchange contributions. The magnitude and energy dependence of the cross sections are approximately reproduced, but the theory fails to describe the angular dependence and the cross section ratios.

I. INTRODUCTION

Photonuclear reactions in the $E_\gamma \gtrsim 100$ MeV region are of interest because these processes, induced by a well-understood probe, are sensitive to meson exchange and isobar effects in nuclear dynamics. The large mismatch between the momentum of the photon and the ejected nucleon implies that the probability of a direct, single-particle knockout process is small. For example, a 300 MeV/c photon ejects a 640 MeV/c proton at 90° in the ^{4}He(γ,p)^{3}H reaction. In the photodisintegration of the deuteron, the importance of meson exchange currents (MEC) and isobar degrees of freedom is well established at energies below the pion production threshold.[1] At higher energies and in more complex nuclei, where MEC and isobar configurations are likely to make significant contributions to photoreactions, no generally accepted framework for treating these effects exists. Part of the difficulty in understanding photonuclear reactions in this energy region stems from a lack of data, in particular (γ,n) data to complement the more easily obtained (γ,p) data. Since the direct, one-body amplitudes are very different for the two reactions, the prediction of both cross sections provides a detailed test of any theory.

Very few data have been published which permit a comparison between the exclusive (γ,p) and (γ,n) reactions at energies above the pion production threshold. There are several measurements of the ^{4}He(γ,p)^{3}H cross section,[2,3,4] as well as one very limited measurement[3] of that for ^{4}He(γ,n)^{3}He. Some measurements of the energy and angular dependence of the ^{16}O(γ,p)^{15}N cross section in the 100 to 400 MeV region have also been reported.[5,6] At energies below the pion threshold, (γ,p) data are available for various nuclei. The ^{12}C(γ,n)^{11}C and ^{16}O(γ,n)^{15}O cross sections between 60 and 160 MeV have been measured[7] and compared with the corresponding (γ,p) results.[8,9] Comparison has also been made[10] between the reactions ^{7}Li(γ,$n_0 + n_2$) and ^{7}Li(γ,p_0) for 60 MeV $< E_\gamma <$ 120 MeV. It is clear from these investigations that the (γ,p) and (γ,n) exclusive cross sections are of comparable magnitude, and both reactions have forward-peaked angular distributions.

These results have been interpreted in terms of phenomenological models for exclusive (γ,N) reactions in which the photon is absorbed by a neutron-proton pair (the so-called quasi-deuteron mechanism) and one of the outgoing nucleons is then rescattered or reabsorbed by the recoiling nucleus. Noguchi and Prats[11] consider the ^{4}He(γ,N) reactions for $E_\gamma < 170$ MeV in such a model. Schoch[12] uses a similar model to describe the ^{16}O(γ,p)^{15}N process for 60 MeV $< E_\gamma <$ 400 MeV, as well as the ratio of the (γ,p) to (γ,n) cross sections in ^{16}O and ^{12}C at 60 MeV. Sené *et al.*[10] compare the predictions of this model with their measurements of the ^{7}Li(γ,N) cross sections. These efforts have had some success in reproducing the trends of the observed cross sections but do not lead to a fundamental understanding of the photonuclear reaction mechanism.

Microscopic calculations of the (γ,N) cross sections must include both the one-body (direct knockout) amplitude and two-body effects such as nucleon-nucleon correlations, MEC, or intermediate-state $\Delta(1232)$ excitation. Distorted-wave–impulse-approximation calculations of the direct amplitude generally underestimate the measured (γ,p) cross sections above $E_\gamma \approx 100$ MeV (Ref. 13) and, more significantly, fail to explain the similar magnitude and forward peaking of the (γ,n) cross sections. Interest therefore centers on which two-body mechanisms should

be introduced into a description of the (γ,N) process and how this should be done.

The contribution of nucleon-nucleon correlations to the (γ,p) and (γ,n) cross sections has been examined in various theoretical treatments.[14–19] A self-consistent random-phase approximation calculation with intermediate excitation of giant resonance states is moderately successful in reproducing the (γ,p) and (γ,n) data for ^{12}C and ^{16}O below 100 MeV.[17] This work has not been extended to higher energies. A model which is similar in formalism and does consider higher energies is that of Gari and Hebach.[18,19] They calculate (γ,N) cross sections, including meson exchange effects, in a gauge-invariant framework while maintaining orthogonality between initial and final states. In this theory the similarity of (γ,n) and (γ,p) processes arises from the dominance of the two-body terms in the transition matrix. In the 100–400 MeV energy region, excitation of the $\Delta(1232)$ resonance would also be expected to be important and perhaps dominant as shown by the calculations of Londergan and Nixon for the ^{16}O(γ,p)^{15}N reaction.[20] Nonresonant pion exchange terms were included in a calculation for ^{4}He by Finjord,[21] while Laget[22] has pointed out that N'(1470) admixtures to the ^{4}He ground state wave function can have large effects. It has been suggested that even explicit quark degrees of freedom may be needed.[23]

In this paper we present differential cross sections for the reactions ^{4}He(γ,n)^{3}He and ^{4}He(γ,p)^{3}H at nucleon angles close to 60°, 90°, and 120° in the center-of-mass frame for photon energies between 100 and 360 MeV. The experimental technique is discussed in Sec. II and the analysis of the data is described in Sec. III. In Sec. IV the data are compared with the theoretical predictions of Gari and Hebach,[19] who have performed the most detailed calculations for these reactions.

II. EXPERIMENTAL PROCEDURE

The data reported here were obtained at the MIT-Bates Linear Accelerator Laboratory. Differential cross sections for the two-body ^{4}He photodisintegration reactions, ^{4}He(γ,p)^{3}H and ^{4}He(γ,n)^{3}He, were measured by detecting the recoiling $A=3$ nuclei. Thus, in both cases charged particles were observed, allowing the same apparatus to be used for both measurements with only minor changes in the electronics. The detected particles were momentum analyzed with the 900 MeV/c spectrometer,[24] which was instrumented with a drift chamber[25] to measure particle position in the dispersion direction and a set of detectors that provided an event trigger and particle identification information. Recoil nuclei were detected at the laboratory angles 46.5°, 72°, and 101°, which correspond to nominal nucleon center-of-mass angles 120°, 90°, and 60°, respectively. The following sections describe the apparatus and experimental method in more detail.

A. Photon beam

Bremsstrahlung photons were produced by an electron beam incident on a 239 mg cm^{-2} ($\sim$0.04 radiation length) tungsten radiator. The beam current was monitored several meters upstream of the target by two nonintercepting current transformers whose gated output was integrated to yield the total charge delivered in a given measurement. These two independent devices were calibrated with a current loop to 0.1% accuracy[26] and yielded results which agreed within 0.5% under experimental conditions. The full, uncollimated bremsstrahlung flux passed through a cooled ^{4}He gas target cell centered 10 cm downstream from the radiator (see Fig. 1). In this arrangement the energy-degraded electron beam also passed through the target, and about one-third of all events were produced by electrodisintegration. However, as discussed in Sec. III, the cross sections extracted from the electrodisintegration contribution were in good agreement with the real photon cross sections.

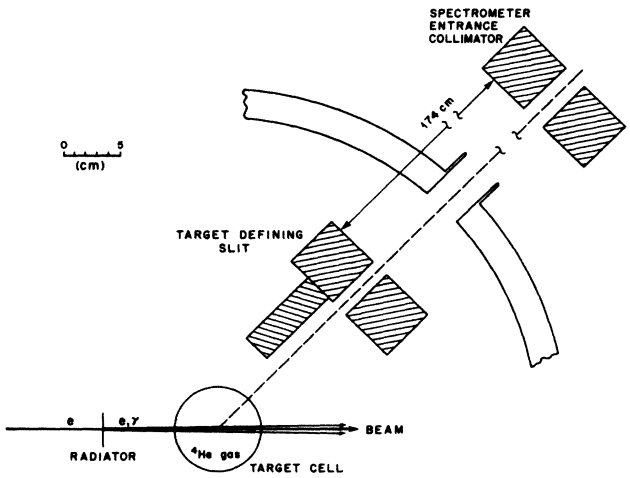

FIG. 1. Arrangement of the target cell, target-defining slit, and bremsstrahlung radiator in the scattering chamber, and the spectrometer entrance collimator.

B. Gas target

The ^{4}He target gas was contained in a cylindrical cell of diameter 7.6 cm and height 6.2 cm with 0.03 mm thick Elgiloy[27] metal walls. Stainless steel top and bottom flanges brazed to the walls provided support for the cooling coils and gas filling pipe (with connection to a pressure gauge) at the top of the cell and a temperature-sensing resistor inside the cell at the bottom. The entire cell, except for the beam entrance and exit regions, was wrapped in aluminum-coated Mylar insulation foil to reduce the radiative heat input from the surrounding scattering chamber. With the beam on the target the gas temperature was about 34 K and the pressure was 0.66 MPa.

An accurate determination of the density of the target gas was made with the beam off by measuring the temperature and pressure after equilibrium was established. The density, typically 2.0 moles/liter, was calculated using a published parametrization of the helium equation of state.[28] The calibration of the temperature sensor was checked[29] by measuring the pressure and temperature at the liquid-gas phase boundary of deuterium and comparing with published results. The target was filled several times during the experiment, and density measurements

made before and after data taking agreed within ±0.5%. The overall accuracy of the density determination was ±2.5%.

A correction for local density fluctuations caused by beam heating of the gas was determined from measurements of particle yield as a function of average beam current. Measurements with different peak currents, pulse lengths, and pulse repetition rates showed that the local gas density was a function only of the average current. The correction for this effect was typically 3%.

C. Spectrometer and detection system

The spectrometer solid angle and the effective target volume were defined by the spectrometer entrance collimator located 194 cm from the target and an additional 5.1 cm thick tungsten slit centered at 17.8 cm from the target center (see Fig. 1). With this arrangement the spectrometer did not see particles originating in the target walls illuminated by the beam. The product of target length and solid angle was evaluated by a straightforward numerical integration procedure.[30] For the laboratory angles 46.5°, 72°, and 101°, the results were 3.72, 2.84, and 2.75 cm msr, respectively, with an estimated error of 1.5%.

The detectors used with the spectrometer comprised a position-sensitive drift chamber in the focal plane, followed by two gas proportional counters for detecting short-range, heavily ionizing particles, and a telescope of five plastic scintillators[31] which detected less heavily ionizing particles (see Fig. 2). The spectrometer momentum acceptance of about 5% was defined by the effective length of the drift chamber.

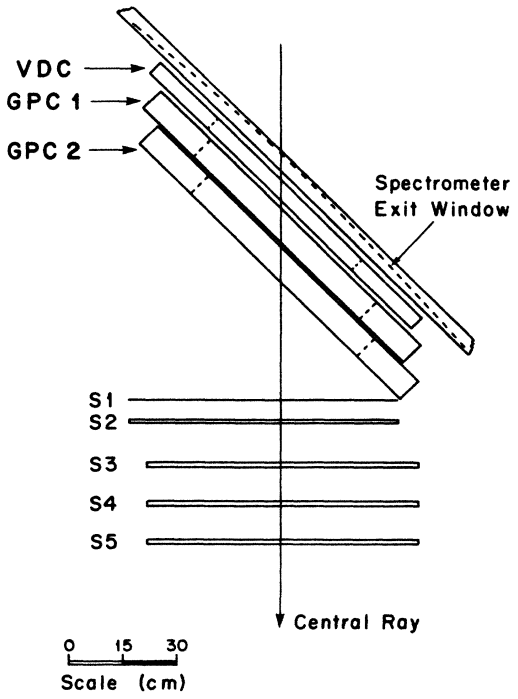

FIG. 2. Arrangement of detectors used with the 900 MeV/c spectrometer. These are a multiwire drift chamber (VDC), two gas proportional counters (GPC1 and 2), and five plastic scintillation counters (S1–5) with thicknesses of 1.59, 3.18, 12.7, 12.7, and 12.7 mm, respectively.

At a given spectrometer field the appropriate trigger logic was determined from the calculated energy loss and range of the particles in all layers of material in the detectors. Examination of the observed energy-loss spectra verified that this calculation was accurate. The trigger logic needed only minor modifications to accommodate changes in the energy and type (^{3}H or ^{3}He) of particle detected. Tritons and ^{3}He particles of the same magnetic rigidity have energies which differ by a factor of 4 and were easily distinguished on the basis of their range in the detectors. Deuterons and ^{3}He's whose energies differ by a factor of 2 have very similar ranges, but could be distinguished by their different energy losses in elements of the detector system. The range of the protons was always greatest and the majority of these events could therefore be vetoed on-line. Without this veto, the relative numbers of protons, deuterons, and ^{3}He's were typically 800:60:1.

D. Gas proportional counters

Extending the ^{4}He(γ,n) measurements to low photon energies required the detection of ^{3}He particles of as low an energy as possible. Two multiwire gas proportional counters were built[30] to detect these heavily ionizing, short-range particles. The thickness of each counter was 14.7 mg cm^{-2}, and each had sufficient energy resolution to separate deuterons from ^{3}He's for ^{3}He kinetic energies between 40 and 80 MeV.

The active area of each counter was 76×36 cm^2, and they had uniform gain over the central 66×20 cm^2 region. The wire spacing was 0.51 cm and the anode-cathode gap was 2.54 cm. These parameters were chosen to produce a large energy loss while minimizing gain variations due to wire positioning errors. Stainless steel wire of 20 μm diameter was used to minimize local gain fluctuations due to wire nonuniformity. The chambers were filled with a mixture of 50% argon and 50% isobutane. The anode pulses from all the wires were combined to form the output signal, and the energy resolution was limited by noise picked up on all wires. Good electrical shielding with external conducting foils was therefore important. The operating voltage was limited to less than 8.1 kV by the onset of photoionization at the cathode which resulted in periodic avalanches. The counters were mounted parallel to the spectrometer focal plane, which is at 45° with respect to the direction of the incident particles (see Fig. 2), so that approximately ten wires were hit by each track. This served to average over the gain variations among the wires. Each counter exhibited a timing jitter of 35 ns due to the variation in drift time of the earliest arriving charge.

Figure 3 illustrates the typical particle identification capability of these counters for particles with the same magnetic rigidity as 41 MeV ^{3}He's. It is seen that the ^{3}He particles are well separated from the deuterons. In this example the event trigger was provided by a coincidence between the two proportional counters. At spectrometer

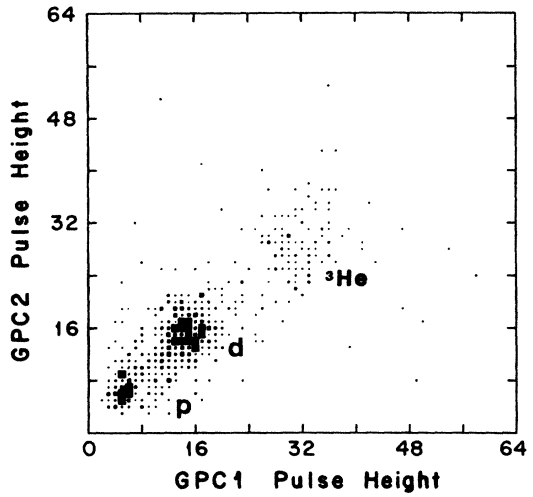

FIG. 3. Correlated pulse height spectra in the two gas proportional counters with the spectrometer field set for 41 MeV ^{3}He particles. The event trigger in this example was provided by a coincidence between the proportional counters. Most of the protons have been suppressed by an on-line veto. The sizes of the symbols indicate the relative numbers of events.

field settings for which scintillators could be included in the trigger, the separation of particle types was superior to that shown in Fig. 3.

E. Data acquisition procedure

Data were taken at bremsstrahlung endpoint (electron) energies of 165, 200, 265, 300, and 365 MeV to investigate the photon energy range from 100 to 360 MeV, though coverage was not complete at all angles due to time and detector limitations. At each electron energy the energy spectra of the $A=3$ recoil nuclei were measured over the range corresponding to the top 120 MeV of the bremsstrahlung spectrum. The two-body kinematic relations could therefore be used to determine uniquely the energy of the bremsstrahlung photon initiating each event since three-body final states containing pions are energetically excluded.

In the measurements performed with the radiator in the electron beam, the observed events were produced in the ratio of approximately 2:1 by bremsstrahlung (real photons) and electrodisintegration (virtual photons). Measurements with the radiator out of the beam were therefore made at about half of the total number of spectrometer field settings to determine the virtual photon contribution to the yield. Taking data with the radiator both in and out at each field setting would have allowed a direct subtraction of the electrodisintegration yield. However, to save time and to make better use of the data, we adopted the alternative method of including a calculated virtual photon spectrum in the effective total photon spectrum for the radiator-in measurements and analyzing these data using this composite spectrum. This procedure is described in detail in Sec. III C.

The background contribution from an empty target cell was measured at several spectrometer field settings with the radiator both in and out of the beam.

III. TREATMENT OF THE DATA

A. Event selection and photon energy calculation

In the analysis procedure, $A=3$ particles were selected by examination of the correlated pulse height spectra from the appropriate combinations of at least two trigger detectors. The position of each particle in the focal plane was then converted to a momentum using the spectrometer calibration discussed below. The particle energy was corrected for the average energy losses in the target gas and the target cell wall. In the worst case, 40 MeV ^{3}He particles suffered an average total energy loss of approximately 7 MeV. This corrected particle energy was used to calculate the photon energy for each event. Variation in the energy loss due to straggling and differing path lengths through the target gas produced a corresponding uncertainty in the calculated photon energies. The typical photon energy resolution due to these effects was ± 3 MeV for the (γ,n) results and always better than ± 1.8 MeV for the (γ,p) results.

The momentum calibration and dispersion of the spectrometer were determined from electron scattering data. At momenta higher than those available in electron scattering, the calibration was extended as described in Ref. 5 using protons of calculable momentum at the endpoint of the spectrum from the $^{16}O(\gamma,p)^{15}N$ reaction. The uncertainty in the photon energy due to the uncertainty in these calibrations was about ± 1.0 MeV. A larger effect was caused by the uncertainty in the electron beam energy, as determined by the beam analysis magnets, which was approximately 2% during this measurement. These two effects contributed a total uncertainty of $\pm 5\%$ in the cross sections.

B. Corrections to the data

The measured particle yields were corrected for events lost due to the rate limitation of the data acquisition system and for the drift chamber inefficiency. Complete information on the first event occurring in each beam burst was stored in the computer, and only the total number of additional events in the burst was recorded. The correction made for this loss was typically 5% and never larger than 14%. The drift chamber had an effective dead time of 300 ns, and if an additional event trigger occurred within this time, both events were rejected. Also, the drift chamber readout was affected by background particles which did not themselves produce a trigger. This resulted in ambiguous position information for some events which were therefore discarded. The correction made for these losses was typically 3% and never larger than 16%.

Background contributions to the particle spectra, determined from target-empty measurements using the same particle identification criteria as in the corresponding target-full measurements, were typically near 5% and never exceeded 15%. The uncertainty in the background contributed only $\pm 1\%$ to the overall systematic uncertainty in the results.

The reduction in detection efficiency for $A=3$ particles which would occur if they picked up atomic electrons before entering the spectrometer or detectors was negligible

at the particle energies in this experiment.[32] Estimates of multiple scattering in the target, slits, and detectors indicated that losses due to these effects were insignificant.

C. Determination of the photodisintegration cross sections

The measured particle momentum spectra were converted to photodisintegration cross sections as a function of real or virtual photon energy by dividing by the appropriate Jacobians and the corresponding calculated photon spectrum. With the radiator in, the primary contribution to the photon spectrum was bremsstrahlung from the radiator, which was calculated taking into account the energy spread of the incident electrons and energy losses due to radiative and collisional processes. Bremsstrahlung contributions from the target wall (5% of the total) and the target gas (less than 1%) were also included, but without considering further electron straggling. The calculations of the photon spectrum (believed to be accurate to $\pm 3\%$) and straggling effects followed Refs. 33 and 34. This formulation of the bremsstrahlung spectrum has been found to be in good agreement with other calculations for photon energies more than 10 MeV below the endpoint.[35] The electrodisintegration contribution to the yield was treated by including a calculated virtual photon spectrum in the total effective photon spectrum. The formalism of Tiator and Wright[36] was adopted for the virtual photon spectrum using the "exact" integral according to the algorithm of Tiator.[37] This represents an improvement over the commonly used formalism of Dalitz and Yennie[38] since the kinematics of the final state is now treated without approximation. The resulting spectrum depends on the angle at which the detected particle is emitted, and the angular dependence is significant for light targets where recoil energies are large. For ^{4}He the Tiator-Wright and Dalitz-Yennie spectra differ by about 10% in the energy region covered in this experiment.

To check the validity of the virtual photon calculation, data were taken with the radiator out at about half of the spectrometer field settings. In these data the virtual photon contribution to the spectrum is dominant, with only a small contribution from bremsstrahlung in the target. In almost all cases the cross sections deduced from the radiator-in and radiator-out measurements agreed, within the statistical accuracy of the data, for photon energies as much as 120 MeV below the endpoints.[30] The only significant discrepancy was observed in one series of (γ,p) measurements at 120° with electron energy 200 MeV, in which the radiator-out cross sections were found to be $\sim 35\%$ larger than the radiator-in cross sections. Although the reason for this difference is not known, it is not thought likely to signify an error in the assumed virtual photon spectrum (see Ref. 30). From the general consistency of the radiator-in and radiator-out data, it is estimated that the systematic uncertainty in the cross sections due to the virtual photon calculation is $\pm 5\%$.

The agreement among cross sections derived from measurements at different electron energies was also examined.[30] For the radiator-in measurements the agreement was always very good for photon energies more than 10 MeV below the endpoints, thus confirming the assumed shape of the bremsstrahlung spectrum. A more limited check on the shape of the virtual photon spectrum was provided by a single comparison of the cross sections at one virtual photon energy obtained from two radiator-out measurements at different electron energies.

IV. RESULTS

The two-body photodisintegration cross sections for ^{4}He derived from this experiment are shown in Figs. 4 and 5 (solid circles) and are listed in Tables I and II. The data are presented in 10 MeV photon energy bins wherever possible; this bin width is larger than [or, at the extreme low-energy end of the (γ,n) measurement, comparable to] the intrinsic photon energy resolution of the ex-

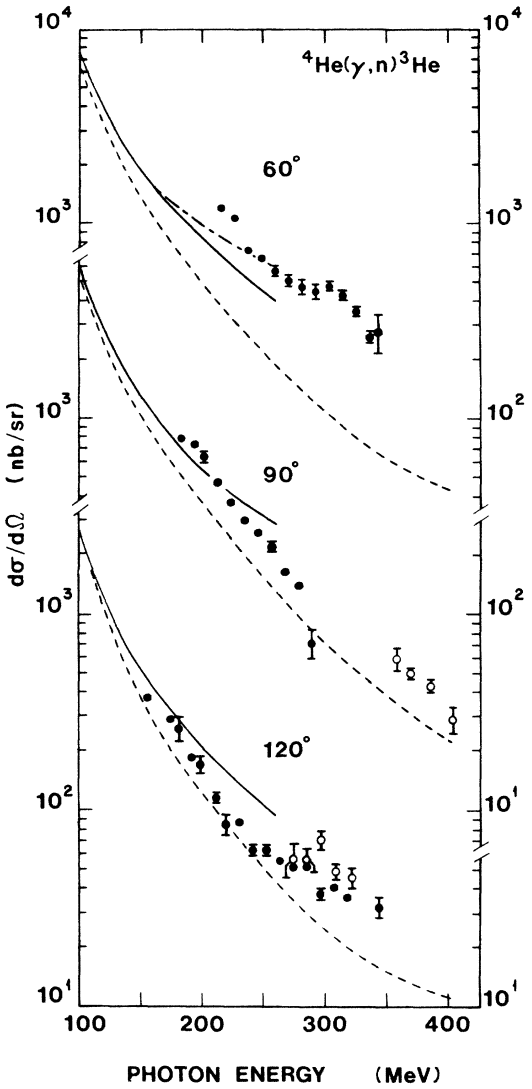

FIG. 4. ^{3}He$(\gamma,n)^3$He cross sections at nucleon center-of-mass angles 60°, 90°, and 120°. Solid circles—this experiment; error bars are statistical. Open circles—Saclay (Ref. 3). The curves represent calculations of Gari and Hebach (Refs. 19 and 41): dashed curve—direct term plus fixed range MEC terms; solid curve—variable range MEC, NN correlation terms, and center-of-mass corrections added; dot-dashed curve—Δ(1232) current added.

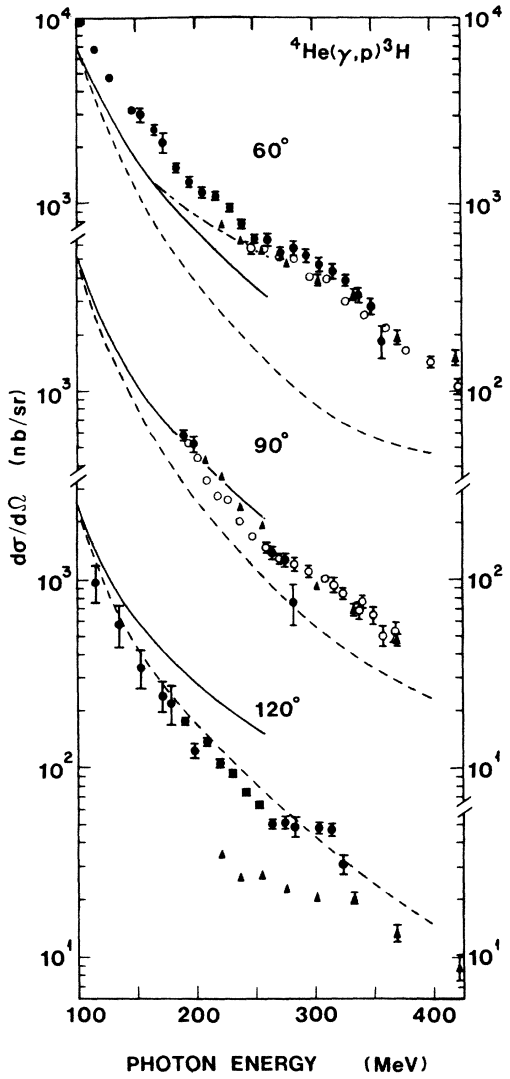

FIG. 5. ^{4}He(γ,p)^{3}H cross sections at nucleon center-of-mass angles 60°, 90°, and 120°. Solid circles—this experiment; error bars are statistical, except for the five lowest energy data at 120° (see the text). Open circles—Saclay (Ref. 3). Triangles—Bonn (Ref. 2). The theoretical curves have the same meaning as in Fig. 4.

periment. Overlapping measurements made with different endpoint energies have been combined, as have the radiator-in and radiator-out measurements. The exact nucleon center-of-mass angles are included in the tables; the plotted cross sections have not been adjusted to correspond to the nominal nucleon angles of 60°, 90°, and 120°. The errors given are purely statistical. The uncertainties discussed previously, together with estimated uncertainties in the radiator thickness and integrated beam current, yield a total systematic uncertainty of ±9%.

The cross sections for the (γ,p) and (γ,n) reactions are seen to be very similar. The trend of the data is to fall smoothly with increasing photon energy, and both cross sections are forward peaked. In both the (γ,p) and (γ,n) results at 60°, there is a suggestion of a bump near 300 MeV.

TABLE I. Differential cross sections in the center-of-mass frame for the ^{4}He(γ,n)^{3}He reaction at nominal nucleon angles 60°, 90°, and 120°. The quoted errors are statistical; the additional systematic uncertainty is ±9%.

E_γ bin (MeV)	θ_n (c.m.) (deg)	$d\sigma/d\Omega$ (c.m.) (nb/sr)
	$\theta_{^3He}$ (lab) = 101.0°	
215±5	62.2	1189 ±42
226±5	61.9	1060 ±42
237±5	61.6	725 ±30
248±5	61.2	659 ±29
259±5	60.9	568 ±36
270±5	60.6	506 ±35
281±5	60.3	468 ±41
292±5	60.0	445 ±41
303±5	59.7	474 ±27
314±5	59.4	424 ±25
325±5	59.1	352 ±20
336±5	58.9	259 ±19
343±1	58.7	275 ±62
	$\theta_{^3He}$ (lab) = 72.0°	
183±5	92.8	786 ±28
194±5	92.4	733 ±24
202±2	92.1	630 ±43
213±5	91.8	468 ±19
224±5	91.5	368 ±17
235±5	91.1	299 ±12
246±5	90.8	258 ±12
257±5	90.5	220 ±13
268±5	90.2	163 ±8
279±5	89.9	140 ±8
289±4	89.6	71 ±12
	$\theta_{^3He}$ (lab) = 46.5°	
155±5	122.6	372 ±9
174±5	122.1	290 ±13
181±1	122.0	258 ±37
192±5	121.7	185 ±9
199±1	121.5	170 ±18
212±5	121.2	116 ±7
219±2	121.0	85 ±10
230±5	120.8	87.1±4.3
241±5	120.5	62.6±4.1
252±5	120.3	62.9±4.0
263±5	120.0	55.4±2.9
274±5	119.8	51.4±2.7
285±5	119.6	51.7±3.0
296±5	119.4	37.5±2.5
307±5	119.2	40.5±1.9
318±5	118.9	36.0±1.8
344±5	118.5	31.2±3.8

A. Comparison with previous measurements

Data from two previous experiments performed at Bonn[2] and Saclay[3] are compared with the present results in Figs. 4 and 5. The present data generally agree well in shape and magnitude with both the (γ,p) and (γ,n) results from Saclay.[3] At 120° in the (γ,n) case the latter are

TABLE II. Differential cross sections in the center-of-mass frame for the ^{4}He(γ,p)^{3}H reaction at nominal nucleon angles 60°, 90°, and 120°. The quoted errors are statistical; the additional systematic uncertainty is ±9%.

E_γ bin (MeV)	θ_p (c.m.) (deg)	$d\sigma/d\Omega$ (c.m.) (nb/sr)
	$\theta_{^3H}$ (lab)=101.0°	
104±3	66.4	9400 ±270
115±4	65.9	6690 ±170
127±4	65.4	4750 ±120
147±5	64.6	3160 ±80
154±1	64.4	2990 ±250
165±5	63.9	2490 ±150
173±2	63.7	2140 ±260
184±5	63.3	1570 ±90
195±5	62.9	1320 ±90
206±5	62.5	1144 ±74
217±5	62.2	1106 ±56
228±5	61.8	952 ±46
239±5	61.5	785 ±43
250±5	61.2	652 ±36
261±5	60.9	649 ±50
272±5	60.6	550 ±40
283±5	60.2	584 ±50
294±5	60.0	533 ±43
305±5	59.7	476 ±41
316±5	59.4	439 ±40
327±5	59.1	391 ±26
338±5	58.8	329 ±29
349±5	58.6	286 ±29
358±3	58.3	187 ±37
	$\theta_{^3H}$ (lab)=72.0°	
191±5	92.5	582 ±34
199±2	92.3	523 ±50
266±5	90.3	140 ±11
277±5	90.0	128 ±11
284±1	89.8	76 ±19
	$\theta_{^3H}$ (lab)=46.5°	
116±3	123.8	959 ±221[a]
136±4	123.2	575 ±146[a]
154±5	122.7	338 ±78[a]
173±5	122.2	239 ±45[a]
180±1	122.0	218 ±54[a]
192±5	121.7	176 ±8
200±2	121.5	124 ±11
210±5	121.3	138.1±7.4
221±5	121.0	106.2±6.1
232±5	120.7	94.0±4.2
243±5	120.5	74.5±3.3
254±5	120.3	63.9±2.9
266±5	120.0	50.5±3.1
277±5	119.8	51.3±3.9
285±2	119.6	48.9±5.9
305±5	119.2	48.1±3.4
316±5	119.0	47.1±3.5
325±3	118.8	31.3±3.7

[a]These larger errors take into account the discrepancy in this region between radiator-in and radiator-out measurements (see the text).

about 15% higher, but this discrepancy is within the quoted systematic errors. At 60° and 90° the present (γ,p) data are in similarly good agreement with the Bonn results.[2] However, at 120° the present (γ,p) data disagree strongly with those from Bonn, the new results being about twice as large. At this angle the Saclay (γ,n) cross section is 2.5 times larger than the Bonn (γ,p) result; this unexpected ratio provided one of the motivations for the present measurement. It now seems likely that the Bonn (γ,p) cross section is too small. It is implied in Ref. 2 that the forward-angle results, having been obtained with an improved experimental setup, are considerably more reliable than the backward-angle data (see also Ref. 39).

The suggestion of a bump near 300 MeV in the (γ,p) cross section at 60° is not inconsistent with either the Bonn or the Saclay (γ,p) results.

The results of two earlier (γ,p) measurements are not shown in Fig. 5. Kiergan *et al.*[4] measured the ^{4}He(γ,p)^{3}H cross section between 180 and 320 MeV photon energy. These data, within their limited statistical accuracy, are consistent with the present results at all angles. The result of a bubble chamber measurement of Gorbunov[40] for $E_\gamma < 170$ MeV has insufficient energy resolution to allow a meaningful comparison with the present data.

B. Comparison with theory

The ^{4}He(γ,p)^{3}H cross section at 90° has been calculated by Finjord,[21] who obtained a reasonably good fit to the Saclay data[3] in a model where nonresonant pion exchange contributions were dominant. Laget[22] also was able to reproduce the Saclay (γ,p) data at 60° and 90° in a calculation in which the ^{4}He ground state wave function contains a 4% admixture of the N'(1470) resonance. Neither of these calculations has been applied to other angles or to the (γ,n) process.

The only extensive theoretical predictions available for both the ^{4}He(γ,p)^{3}H and ^{4}He(γ,n)^{3}He cross sections in the 100–400 MeV energy region are by Gari and Hebach (GH).[19,41] In their model MEC are introduced by evaluating the gauge contributions represented by the matrix elements of the operator $\Omega=[V,Q^L_\lambda]$, where Q^L_λ are the electric multipole operators. The effective two-body potential, V, which they use, has a Yukawa radial dependence and an isospin structure such that V acts on pn but not on pp or nn pairs. As a result, features such as the approximate equality of the (γ,p) and (γ,n) cross sections necessarily emerge from the GH model since the two-body terms dominate over the one-body terms in the energy range of interest. Effects of initial- and final-state correlations are treated but are found to be small at these energies. GH use orthogonal initial- and final-state wave functions corresponding to the same deep, real potential and are thus unable to take correct account of the distortion of the outgoing nucleons. Resonant Δ(1232) excitation is introduced in an approximate way.

The dashed curves in Figs. 4 and 5 show the predictions of GH which include the small direct knockout term and the dominant MEC contributions calculated with a fixed pion range parameter in the two-body potential. The angular dependence of the theory is clearly incorrect; the

theoretical curve lies far below the data at 60° and is roughly correct only at 120°. Corrections for center-of-mass motion and the energy dependence of the pion range produce large enhancements in the predicted cross sections at all angles, as is illustrated by the solid curves. (Due to the approximations used, the latter corrections could be applied only up to a photon energy of 260 MeV.) However, the theory is still low at 60° and now exceeds the data at 120°. The contribution of intermediate $\Delta(1232)$ excitation was calculated only at 60° and was found to produce a further significant increase in the predictions (dot-dashed curves) in the energy range for which it was evaluated.

Although the treatment of GH does produce roughly equal (γ,p) and (γ,n) cross sections and qualitatively the correct energy dependence for both, the results are far from quantitative agreement with the data. In particular, the predicted angular distribution is not sufficiently forward peaked. This could possibly be due to the form of the two-body potential, V, for which GH use a convenient, simple form without the hard core or tensor part of more realistic interactions. Another choice might significantly alter the angular dependence of the two-body contributions, but this has not been explored. GH emphasize the introduction of the MEC contributions in such a way that both gauge invariance and orthogonality of initial and final states are preserved. The latter choice certainly depresses the direct knockout contribution, and its appropriateness as opposed to using a more realistic final state optical potential has not been thoroughly assessed, although some estimates have been reported.[42]

The slight bump in the $E_\gamma \approx 300$ MeV region seen in the 60° data reported here could be an indication that the $\Delta(1232)$ resonance is playing a role in the ^{4}He photodisintegration process. A calculation by Londergan and Nixon for the $^{16}O(\gamma,p)^{15}N$ reaction[20] suggests that $\Delta(1232)$ excitation produces a major contribution to the cross section in the energy region between 100 and 400 MeV. However, their approach has been criticized by GH,[19] who found that the cross section is dominated by nonresonant MEC and that the $\Delta(1232)$ contribution is generally small.

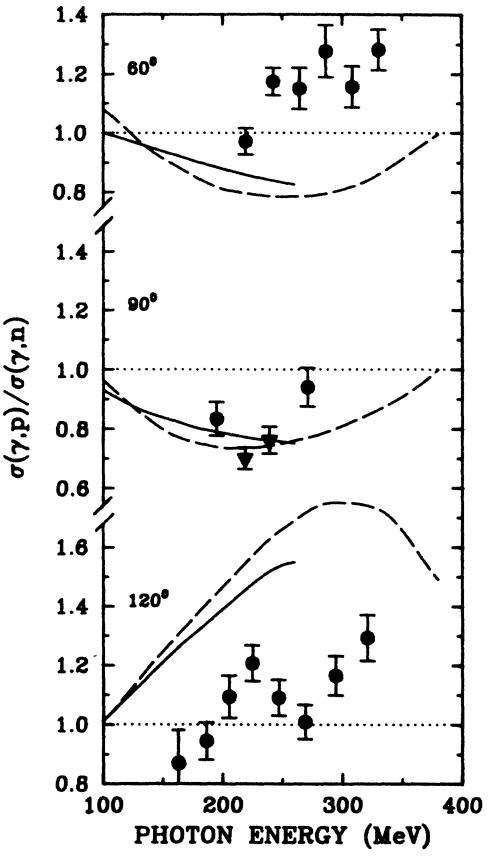

FIG. 6. Ratio of (γ,p) and (γ,n) cross sections at nucleon center-of-mass angles 60°, 90°, and 120°. The solid circles were determined using data from this experiment only. The systematic uncertainty in these points is ±2%. The triangles represent ratios obtained from the present (γ,n) data and the Saclay (γ,p) data at 90° (Ref. 3), since at these energies the (γ,p) cross section was not measured in this experiment. The Saclay cross sections were multiplied by 1.04 to match the present (γ,p) data near 200 and 240 MeV. The theoretical curves have the same meaning as in Fig. 4.

C. Ratio of (γ,p) and (γ,n) cross sections

A useful result of the present experiment is an accurate determination of the ratio, R, of the differential cross sections for the (γ,p) and (γ,n) reactions. The ratio is displayed as a function of photon energy in Fig. 6. Just as the experimental values of R are insensitive to some systematic uncertainties in the measurements, one might expect calculations of R to be less sensitive to some ingredients of the model such as the ^{4}He ground state wave function. Figure 6 shows R to be within 30% of unity at all angles, with slightly greater values at higher photon energies. It is seen that the calculations of GH produce only qualitative agreement with the data. The predicted angular dependence is incorrect, the calculated ratio being smaller at 60° and larger at 120° than the measured ratios, whether or not the corrections to the basic theory are included.

D. Summary and conclusions

The $^4He(\gamma,n)^3He$ and $^4He(\gamma,p)^3H$ reactions have been studied and found to have approximately equal cross sections over a broad range of photon energies and nucleon emission angles. The only structure in the cross sections, which otherwise decrease steadily with increasing photon energy, is a slight bump in the vicinity of 300 MeV in both the (γ,n) and (γ,p) results at 60°.

The data are compared with a calculation by Gari and Hebach[18,19,41] which attributes most of the cross section to MEC amplitudes. Although the order of magnitude of the measured (γ,p) and (γ,n) cross sections is approximately reproduced, the energy and angular dependence is not successfully predicted. However, this theory does offer an explanation of the approximate equality between (γ,p) and (γ,n) cross sections, which has until now only been understood at a phenomenological level via the

quasi-deuteron model. This represents a significant step in the theoretical treatment of these reactions. Further theoretical work is clearly needed, and additional measurements of both (γ,p) and (γ,n) cross sections over a wider angular range and for other nuclei would be valuable in improving our understanding of photonuclear reaction mechanisms at intermediate energies.

ACKNOWLEDGMENTS

This work was supported by the U.S. Department of Energy, the U.S. National Science Foundation, and the U.K. Science and Engineering Research Council. R. S. Turley acknowledges the support of the Hughes Aircraft Corporation Staff Doctoral Fellowship.

*Present address: SIN, CH-5234 Villigen, Switzerland.
†Present address: Hughes Research Laboratories, 3011 Malibu Canyon Rd., Malibu, CA 90265.

[1]H. Arenhövel, W. Fabian, and H. G. Miller, Phys. Lett. **52B**, 303 (1974); H. Arenhövel, Nucl. Phys. **A374**, 521c (1982), and references therein.
[2]J. Arends *et al.*, Nucl. Phys. **A322**, 253 (1979).
[3]P. E. Argan *et al.*, Nucl. Phys. **A237**, 447 (1975).
[4]S. E. Kiergan, A. O. Hanson, and L. J. Koester, Jr., Phys. Rev. C **8**, 431 (1973).
[5]M. J. Leitch *et al.*, Phys. Rev. C **31**, 1633 (1985).
[6]R. S. Turley *et al.*, Phys. Lett. **157B**, 19 (1985).
[7]H. Schier and B. Schoch, Nucl. Phys. **A229**, 93 (1974); H. Göringer and B. Schoch, Phys. Lett. **97B**, 41 (1980); H. Göringer, B. Schoch, and G. Lührs, Nucl. Phys. **A384**, 414 (1982).
[8]J. L. Matthews, D. J. S. Findlay, S. N. Gardiner, and R. O. Owens, Nucl. Phys. **A267**, 51 (1976).
[9]D. J. S. Findlay and R. O. Owens, Nucl. Phys. **A279**, 385 (1977).
[10]M. R. Sené *et al.*, Phys. Rev. Lett. **50**, 1831 (1983).
[11]C. T. Noguchi and F. Prats, Phys. Rev. C **14**, 1133 (1976).
[12]B. Schoch, Phys. Rev. Lett. **41**, 80 (1978); Habilitationsschrift, Universität Mainz, 1980 (unpublished).
[13]S. Boffi, C. Giusti, and F. D. Pacati, Nucl. Phys. **A359**, 91 (1981).
[14]W. Weise and M. G. Huber, Nucl. Phys. **A162**, 330 (1971); see also Ref. 8.
[15]M. Fink, H. Hebach, and H. Kümmel, Nucl. Phys. **A186**, 353 (1972).
[16]A. Małecki and P. Picchi, Lett. Nuovo Cimento **8**, 16 (1973).
[17]M. Cavinato, M. Marangoni, P. O. Ottaviani, and A. M. Saruis, Nucl. Phys. **A373**, 445 (1982); M. Cavinato, M. Marangoni, and A. M. Saruis, Nuovo Cimento **76A**, 197 (1983); Nucl. Phys. **A422**, 237 (1984); **A422**, 273 (1984).
[18]M. Gari and H. Hebach, Phys. Lett. **49B**, 29 (1974); Phys. Rev. C **10**, 1629 (1974); H. Hebach, A. Wortberg, and M. Gari, Nucl. Phys. **A267**, 425 (1976).
[19]M. Gari and H. Hebach, Phys. Rep. **72**, 1 (1981).
[20]J. T. Londergan and G. D. Nixon, Phys. Rev. C **19**, 998 (1979).
[21]J. Finjord, Nucl. Phys. **A274**, 495 (1976).
[22]J. M. Laget, Phys. Lett. **55B**, 37 (1975).
[23]L. S. Kisslinger, Phys. Lett. **112B**, 307 (1982).
[24]W. Bertozzi *et al.*, Nucl. Instrum. Methods **162**, 211 (1979).
[25]W. Bertozzi *et al.*, Nucl. Instrum. Methods **141**, 457 (1977).
[26]P. C. Dunn, Nucl. Instrum. Methods **165**, 163 (1979).
[27]Elgiloy Company, Elgin, IL 60120.
[28]S. Angus and K. M. de Rueck, *International Thermodynamic Tables of the Fluid State-4* (Pergamon, Oxford, 1977), p. 35.
[29]B. C. Craft, Ph.D. thesis, Massachusetts Institute of Technology, 1982 (unpublished).
[30]R. A. Schumacher, Ph.D. thesis, Massachusetts Institute of Technology, 1983 (unpublished).
[31]E. R. Kinney *et al.*, Nucl. Instrum. Methods **185**, 189 (1981).
[32]L. C. Northcliffe and R. F. Schilling, Nucl. Data Tables **A7**, 233 (1970).
[33]J. L. Matthews and R. O. Owens, Nucl. Instrum. Methods **111**, 157 (1973).
[34]J. L. Matthews, D. J. S. Findlay, and R. O. Owens, Nucl. Instrum. Methods **180**, 573 (1981).
[35]D. I. Sober *et al.*, Phys. Rev. C **28**, 2234 (1983).
[36]L. Tiator and L. E. Wright, Nucl. Phys. **A379**, 407 (1982); L. E. Wright and L. Tiator, Phys. Rev. C **26**, 2349 (1982); L. Tiator and L. E. Wright, Comput. Phys. Commun. **28**, 265 (1983).
[37]L. Tiator, private communication.
[38]R. H. Dalitz and D. R. Yennie, Phys. Rev. **105**, 1598 (1957).
[39]A. Hegerath, Ph.D. thesis, Universität Bonn, 1978 (unpublished).
[40]A. N. Gorbunov, Phys. Lett. **27B**, 436 (1968).
[41]H. Hebach, private communication.
[42]S. Boffi *et al.*, Nucl. Phys. **A379**, 509 (1982); C. Ciofi degli Atti, M. M. Giannini, and G. Salmè, Nuovo Cimento **76A**, 225 (1983); F. Cannata, J. P. Dedonder, and S. A. Gurvitz, *ibid.* **76A**, 478 (1983); S. Boffi, R. Cenni, C. Giusti, and F. D. Pacati, Nucl. Phys. **A420**, 38 (1984).